TU Delft

Delft University of Technology

Dual-Frequency Subharmonic Ultrasound Contrast Imaging for Non-Invasive Blood Pressure Measurement

Spiekhout, Sander; Voorneveld, Jason; de Jong, Nico; Bosch, Johannes G.

DOI
10.1016/j.ultrasmedbio.2025.01.015

Publication date
2025

Document Version
Final published version

Published in
Ultrasound in Medicine and Biology

Citation (APA)
Spiekhout, S., Voorneveld, J., de Jong, N., & Bosch, J. G. (2025). Dual-Frequency Subharmonic Ultrasound Contrast Imaging for Non-Invasive Blood Pressure Measurement. *Ultrasound in Medicine and Biology*, *51*(5), 870-876. https://doi.org/10.1016/j.ultrasmedbio.2025.01.015

Important note
To cite this publication, please use the final published version (if applicable).
Please check the document version above.

Copyright
Other than for strictly personal use, it is not permitted to download, forward or distribute the text or part of it, without the consent of the author(s) and/or copyright holder(s), unless the work is under an open content license such as Creative Commons.

Takedown policy
Please contact us and provide details if you believe this document breaches copyrights.
We will remove access to the work immediately and investigate your claim.

This work is downloaded from Delft University of Technology.
For technical reasons the number of authors shown on this cover page is limited to a maximum of 10.

Ultrasound in Medicine & Biology 51 (2025) 870–876

Contents lists available at ScienceDirect

Ultrasound in Medicine & Biology

journal homepage: www.elsevier.com/locate/ultrasmedbio

Original Contribution

Dual-Frequency Subharmonic Ultrasound Contrast Imaging for Non-Invasive Blood Pressure Measurement

Sander Spiekhout [a,*], Jason Voorneveld [a], Nico de Jong [a,b], Johannes G. Bosch [a]

[a] Biomedical Engineering, Erasmus Medical Center, Rotterdam, The Netherlands
[b] Department of Imaging Physics, Delft University of Technology, Delft, The Netherlands

ARTICLE INFO

Keywords:
Lipid-coated microbubbles
Ultrasound contrast agents
Blood pressure estimation
Ambient pressure sensitivity
Subharmonic-aided pressure estimation

ABSTRACT

Here we propose an ultrasound contrast-based imaging method that enables non-invasive quantitative assessment of ambient pressure changes inside the body (such as blood pressure). We subject the microbubbles in the contrast agent to two frequencies: A low-frequency (57 kHz) signal that dynamically manipulates the ambient pressure, and a series of high-frequency (4 MHz) pulses for exciting and imaging the bubble response. The imaging pulses exploit the ambient pressure sensitivity of the subharmonic microbubble response, while the low-frequency signal provided an intrinsic calibration for measurement of ambient pressure changes. We tested this approach in an *in vitro* setup and show that it can visualize and quantify ambient pressure differences with a sensitivity of 0.5 dB/kPa.

Introduction

Blood pressure is an important indicator for cardiovascular health, and interstitial fluid pressure is important in cancer diagnosis [1]. The intraluminal pressures inside the different heart chambers and blood vessels are of high importance for assessment of heart function, severity of vascular stenoses, and loading conditions of the heart [2], However, such intraluminal pressures can currently only be measured by invasive means such as catheters and pressure wires, and non-invasive means of measuring these pressures would be highly welcomed, particularly for use as early-stage biomarkers. Ultrasound contrast agents, specifically microbubbles, have been explored for many years as potential non-invasive pressure sensors as the acoustic behavior of the microbubbles is known to be highly dependent on the surrounding fluid pressure.

In contrast-enhanced ultrasound (CEUS), lipid-coated gas-filled microbubbles (diameter 1–10 μm) are administered intravenously and imaged with low acoustic amplitudes. Due to the non-linear properties of the viscoelastic microbubble shell, the effective stiffness and effective resonance of the microbubbles changes drastically with small size changes [3,4], such as those induced by a small ambient pressure difference. The maximum subharmonic scattering – which occurs when the resonance of the bubble matches half the ultrasound driving frequency – changes strongly with ambient pressure [4].

However, the mechanics of coated microbubbles, and hence the subharmonic scattered amplitude, also depend on other factors than ambient pressure. For example, the subharmonic scattering changes over time through dissolution [5,6], and subharmonics are enhanced by the presence of iodinated contrast [7]. Subharmonic sensitivity to ambient pressure, *i.e.*, the slope of the subharmonic as a function of static over-pressure, is also strongly influenced by the acoustic frequency and amplitude [8]. Consequently, the values reported for subharmonic sensitivity to ambient pressure differs substantially across studies, even for well-controlled *in vitro* measurements [8,9].

Despite these dependencies on external factors, the clinical value of non-invasive pressure estimation *via* the subharmonic scattered intensity in CEUS imaging has been demonstrated repeatedly *in vivo* [10–12]. The subharmonic amplitude has been shown to be particularly sensitive to small pressure changes, more so than scattering at other harmonics [8,9]. SubHarmonic Aided Pressure Estimation (SHAPE) [9] has been investigated clinically for its potential to predict the therapeutic response of breast lesions to chemotherapy [12], and for its potential in diagnosing portal hypertension [13]. The subharmonic scattering values over a cardiac cycle also correlate with blood pressure catheter readings [14], which potentially allows qualitative monitoring of variations in pulse pressure. However, the sensitivity of subharmonics to ambient pressure also depends on the pulse shape [15], which suggests that calibration values are uniquely tied to the used ultrasound equipment. Furthermore these calibration values, which are obtained via *in vitro* scattering measurements as a function of static over-pressure, can underestimate the *in vivo* sensitivity [11]. To overcome the limitation of unknown acoustic pressure *in vivo*, SHAPE studies now make use of an optimization scheme that determines the optimal acoustic pressure by

* Corresponding author. Biomedical Engineering, Thorax Center, Erasmus Medical Center, EE-2302, Wytemaweg 80, Rotterdam 3015 CN, The Netherlands.
E-mail address: sanderspiekhout@gmail.com (S. Spiekhout).

https://doi.org/10.1016/j.ultrasmedbio.2025.01.015
Received 11 October 2024; Revised 20 December 2024; Accepted 23 January 2025

0301-5629/© 2025 The Author(s). Published by Elsevier Inc. on behalf of World Federation for Ultrasound in Medicine & Biology. This is an open access article under the CC BY license (http://creativecommons.org/licenses/by/4.0/)

maximizing the sensitivity of the subharmonic intensity to the acoustic pressure, and by extension to the ambient pressure [16].

A more robust calibration procedure could allow quantitative non-invasive pressure measurements *via* subharmonic scattering with great diagnostic value for oncology and cardiovascular disease. The approach we propose here is to apply a low-frequency (kHz range) acoustic wave as a dynamic manipulation of the ambient pressure, similar to what was employed by Faez et al. [17]. Performing regular pulse echo imaging over a dynamically manipulated ambient pressure could, in principle, measure the subharmonic sensitivity to ambient pressure, as shown in the scattering experiment by Faez et al. [17]. In that *in vitro* setup, separate single-element transducers from different angles were used, but this could in principle also be done clinically using a dual-frequency transducer. While dual-frequency CEUS imaging has been used to enhance the contrast-to-tissue ratio [18], here we instead test whether it can provide real-time feedback on the subharmonic sensitivity to ambient pressure [17].

Methods

In this section we describe two different setups employing this dual-frequency approach that we use to characterize the method and validate the results: one that uses cross-propagation of the kHz wave and the imaging waves, and another using co-propagation. The cross-propagating setup directly images dynamically manipulated subharmonic scattering and is also used to optimize for microbubble concentration and acoustic amplitude. The optimized settings are then used in the co-propagating setup, which is closer to the intended imaging implementation, described later, and the results are compared with an externally applied static ambient pressure (SAP).

Cross-propagating setup

The cross-propagating setup consisted of a large water tank around a smaller 800 mL tank that contained the microbubble suspension (*i.e.*, the bubble tank), shown schematically in Figure 1. The open-top bubble tank was continuously stirred magnetically and filled with room-temperature water (left overnight prior to the experiment) and with SonoVue (Bracco Suisse SA, Plan-les-Ouates, Switzerland) microbubbles, of which the filling gas was substituted by C_4F_{10} gas, following the instructions of Kanbar et al. [6]. The distance between the bubble tank and the wall of the water tank was approximately 8 cm. The bubble tank has two acoustic windows (polymethylpentene sheets of 2 mm thickness, see dotted lines in Fig. 1) from which the low-frequency acoustic waves could enter and exit. Because the acoustic impedance of these windows was close to that of water (1.44 [19] and 1.48 MRayl [20], respectively), reflections were negligible.

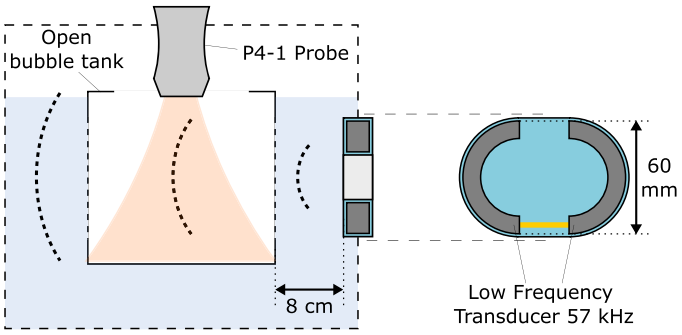

Figure 1. Cross-propagation scattering setup used to optimize for bubble concentration and acoustic amplitude. A large water tank contains a bubble tank that is opened at the top to allow access for the imaging probe. A low-frequency transducer transmits a 57 kHz wave to the bubble tank to dynamically manipulate the ambient pressure.

The dynamic ambient pressure (DAP) was induced by a ring-shaped low-frequency transducer (DH-43 60 × 30 × 10 mm, P4P8 piezoelectric ceramic ring, Shenzhen More-Suns Electronics Co., Ltd., Shenzhen, China). This low-frequency single-element transducer was cut in half, then reconnected electrically and sealed inside a custom holder to allow co-propagation with the imaging probe, see Figure 3. This transducer generated a 57 kHz, 10 cycle pressure wave Gaussian tapered over the first two and last two cycles. The acoustic field of this low-frequency wave was characterized with a hydrophone (TC4038, Teledyne RESON, Slangerup, Denmark) and found to be quite non-homogeneous, with peak-to-peak acoustic pressures ranging from 2 to 10 kPa (15 to 75 mm Hg) in the region of the bubble tank.

The imaging probe (ATL P4-1, Philips Healthcare, The Netherlands) was coupled to a fully programmable Vantage 256 ultrasound system (Verasonics Inc., Kirkland, WA, USA), and its high-frequency transmit burst was delayed by 105 μs with respect to the DAP wave by an external trigger signal to allow the low-frequency wave to reach full amplitude at the imaged location. The imaging probe transmits a 4 MHz, eight-cycle Gaussian-tapered, diverging wave with a pulse repetition frequency (PRF) of 100 Hz. The DAP amplitude was set to 0 for 16 frames after each 16th frame to obtain an equal number of modulated frames and unmodulated frames as a reference, representing the SAP.

Optimizing bubble concentration and acoustic pressure

The subharmonic amplitude was measured while varying the acoustic amplitude and testing the following bubble concentrations: 25, 50, 100, 200 and 400 μL to 800 mL (1×10^4, 2×10^4, 4×10^4, 8×10^4, 16×10^4 microbubbles/mL). For each concentration, the peak acoustic amplitude was swept from 14 to 70 kPa (28–140 kPa peak to peak) in 1.75 kPa steps, and 1280 frames (640 modulated and 640 reference) were recorded at each setting. Recording, storing and subsequently starting the new sequence took approximately 30 s. After this measurement sequence, another measurement sequence was performed on the same microbubble suspension to confirm the microbubble stability. In this second measurement, the pressure was increased from 14 to 26 kPa, as this is where sensitivity was most visible in preliminary measurements, with the same 1.75 kPa step size used. The microbubble suspension was refreshed before each concentration.

Image processing

The recorded radio-frequency data were beamformed once with the full bandwidth, and once with a filter around the subharmonic frequency (1.8–2.2 MHz). The 5 × 32 × 1280 beamformed images were grouped and averaged, such that for each acoustic amplitude and bubble concentration four images were obtained: one unfiltered without DAP (Fig. 2a), one unfiltered with DAP (Fig. 2b), one filtered around the subharmonic without DAP (Fig. 2c), and one filtered around the subharmonic with DAP (Fig. 2d). The diagonal stripes in the modulated subharmonic image (Fig. 2d) are a direct manifestation of the microbubbles' subharmonic sensitivity to the DAP, which was not visible in the fundamental signal nor in the reference images, see Figures 2a–c. These stripes are diagonal because the low-frequency wave traverses the imaging plane in a lateral direction at the same speed of sound as the imaging wave traverses it axially [21]. The subharmonic intensity variation in axial direction was extracted in the frequency domain to find the optimal acoustic imaging amplitude and microbubble concentration. Note that this subharmonic intensity variation (dB), in principle, could be used as a measure of the sensitivity (dB/kPa). However, as the applied DAP amplitude varied considerably over the imaged area, and, also considering that the intensity variation from the DAP was not compared with a SAP change in this experiment, the exact subharmonic intensity variation was not considered a meaningful measure for the sensitivity to ambient pressure. One should also note that because of noise, the change in subharmonic intensity did not go down to 0 dB completely.

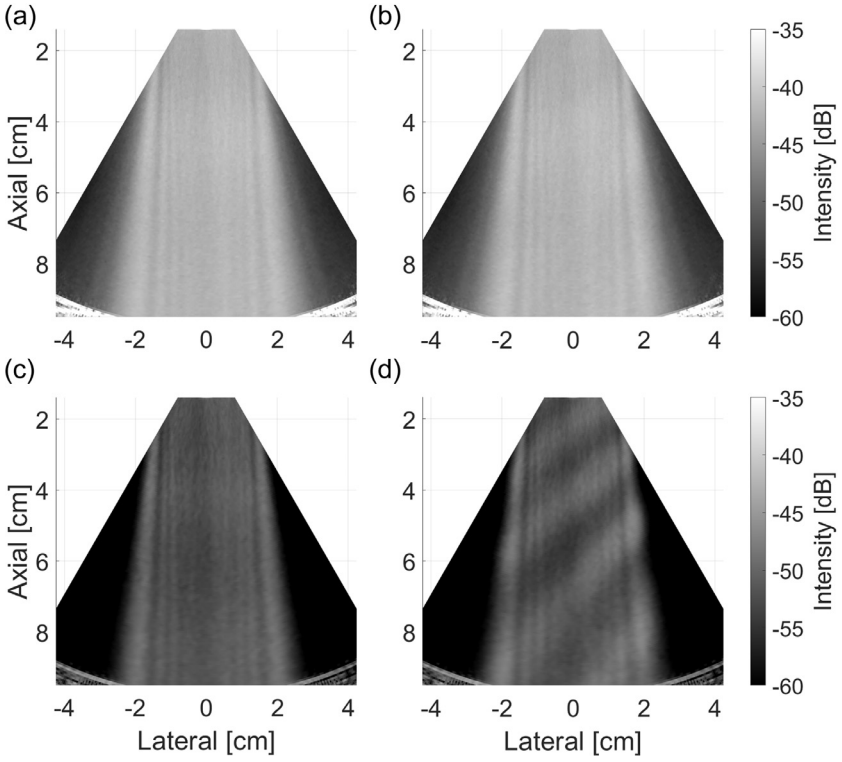

Figure 2. Averaged B-mode images from the cross-propagating experiment from the fundamental radio-frequency (RF) data (a) without dynamic ambient pressure (DAP) modulation, and (b) with DAP modulation. B-mode images for the subharmonic filtered RF data (c) without DAP modulation and (d) with DAP modulation.

Co-propagation setup

This setup was used to test whether the sensitivity measured from the DAP manipulation matched the measured sensitivity in case of a change in SAP (Fig. 3). It consisted of the same large water tank around a sealed bubble tank that contained the room-temperature bubble suspension and a slice of tissue-mimicking material. This bubble tank can be pressurized with a cuff pump equipped with a manometer (Heine Gamma G5; Heine Optotechnik, Herrsching am Ammersee, Germany). The applied pressures from the cuff pump were confirmed separately with a Delta-Cal (Utah Medical Products, Salt Lake City, UT, USA). The closest wall of the bubble tank was placed approximately 9 cm from the dual-frequency transducer, which was mounted on an acoustic window on the outside of the large water tank. This dual-frequency transducer consists of a low-frequency transducer and a P4-1 imaging probe, both placed inside the custom holder. In this manner the low-frequency wave and imaging wave co-propagate, with the resulting pressure in the image, *i.e.*, the instantaneous ambient pressure, the sum of the SAP and the DAP [18]. By varying the phase offset of the DAP wave with respect to the imaging pulse, the resulting instantaneous ambient pressure can be varied per image. As the DAP field was not homogeneous over the entire imaged frame, a smaller region of interest (ROI; 1.5 × 1 cm) at a depth of 130 mm, as indicated in Figure 3, was selected. The DAP amplitude in this ROI was 5.4 ± 0.4 kPa peak to peak (corresponding to 40 ± 2.9 mm Hg).

The eight-cycle, 4 MHz imaging pulse was transmitted with a PRF of 100 Hz, with a fixed 38 μs delay from the start of the DAP using an external trigger signal to account for the slower amplitude response of the low-frequency (LF) transducer. Sixteen modulated frames were followed by 16 unmodulated frames, and an additional delay of one tenth of the low-frequency wavelength (1.75 μs) was programmed after each group of 32 frames. After 320 frames the additional delay was reset to zero, and this entire sequence was repeated four times, which resulted in

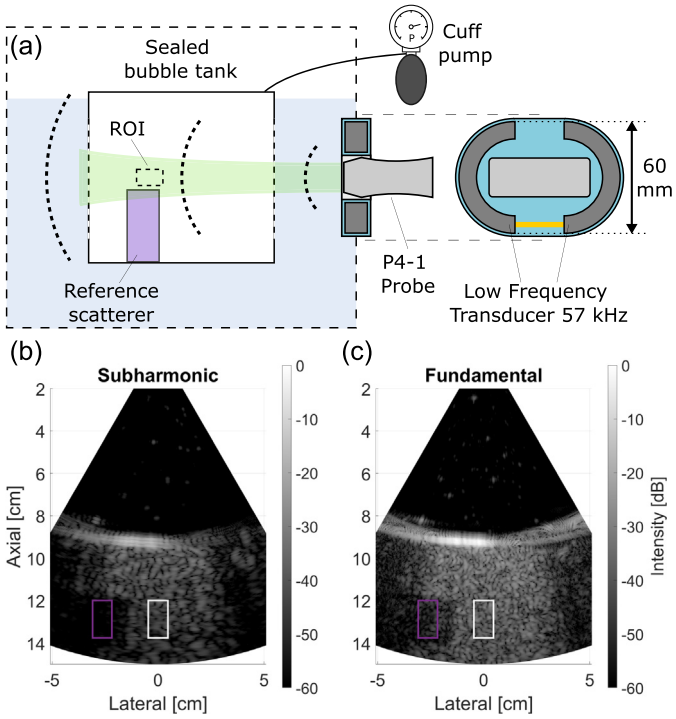

Figure 3. (a) Setup used for the co-propagation experiment. The sealed bubble tank is imaged through an acoustic window using the combined dual-frequency transducer. The tank is pressurized using a cuff pump and a slice of tissue-mimicking material provides a linearly scattering reference. (b) Example frame from the subharmonic signal and (c) example frame from the fundamental signal with the region of interest used for the measurement is shown by white boxes, and the reference scatterer is shown by purple boxes. ROI, region of interest.

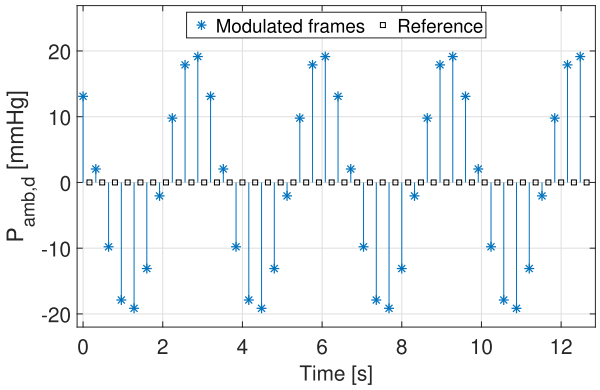

Figure 4. Timing diagram used for the imaging sequence. The blue stars correspond with 32 recorded frames at the indicated dynamic ambient pressure (DAP)-modulated level, and the black squares correspond with 32 recorded frames without DAP modulation.

capturing frames with instantaneous ambient pressures that corresponded with the diagram in Figure 4. The total sequence recorded at each SAP setting encompassed 1280 frames (4 × 320) recorded over 12.8 s. Of these 1280 frames, 640 were DAP modulated and 640 were unmodulated control frames.

Subharmonic response to a static and DAP change

The co-propagation setup (Fig. 3) was used to compare the effect of a change in SAP with the effect from DAP on subharmonic scattering from the diluted microbubble suspension. The acoustic imaging pressure was set to 70 kPa for this experiment. The bubble tank was filled with an aqueous microbubble solution at a concentration of 8×10^4 MBs/mL. The bubble tank was then sealed and placed in the water tank, where it was continuously stirred and set to rest for 2 min. After the bubbles settled, the first measurement sequence was recorded, then the SAP was adjusted and the next sequence was recorded until all 31 SAP levels were recorded. Recording, storing and adjusting the SAP took 25 s for each step. SAP levels were first increased by 20 mm Hg up to a maximum of 100 mm Hg over pressure, and subsequently decreased by 20 mm Hg increments down to 0 mm Hg over pressure. This SAP cycle was repeated three times on the same bubble suspension (31 measurements in total). This protocol allowed us to assess whether hysteresis effects occur by comparing subharmonic behavior during increasing and decreasing SAP, and allowed assessment of whether the subharmonic behavior is reversible over consecutive pressurization cycles. This entire measurement procedure was repeated five times using a fresh microbubble suspension.

The recorded frames were beamformed and averaged once with a bandpass filter around the fundamental (3.8–4.2 MHz), and once with the radio-frequency data filtered around the subharmonic (1.8–2.2 MHz). From these beamformed images, the intensity from the 1.5 × 1 cm ROI was extracted as a measure of the subharmonic and fundamental intensity (white boxes in Fig. 3), and the intensity from the tissue-mimicking material was extracted as a reference (purple boxes in Fig. 3). The relative subharmonic intensity was then determined by dividing the subharmonic by a fixed value.

Results

Optimizing subharmonic sensitivity to DAP

The subharmonic intensity for four microbubble concentrations and varying acoustic pressures is shown in Figure 6. The variation in subharmonic intensity was determined as a function of acoustic imaging pressure for the five tested microbubble concentrations. The recordings from the first four concentrations all showed a maximum change in subharmonic intensity around 2.5 dB compared with the 0.5 dB noise level (Fig. 5a). The subharmonic intensity change for the highest MB concentration (16×10^4) never exceeded 1 dB, and was therefore not included in Figure 5. The acoustic amplitude at which the maximum subharmonic intensity occurred increased with MB concentration, indicating that attenuation played a role. At 50 kPa all of the four lower MB concentrations showed a subharmonic intensity change of at least 2 dB.

The subharmonic intensity change of the first (solid stars) and second (empty squares) acoustic pressure sweep are plotted for the lower three MB concentrations in Figures 5b–d. This shows that after the first pressure sweep, similar subharmonic intensity changes in response to the DAP can be measured. The subharmonic intensity change over this acoustic amplitude range generally increased, and the change could already be observed at a low acoustic amplitude of 16 kPa. This indicates that the microbubbles were stable in the solution. The slight increase in subharmonic intensity change may have resulted from gas diffusion during the approximately 15 min duration in-between sweeps, which is known to increase subharmonics [7].

Subharmonic sensitivity to static and DAP

The 8×10^4 MBs/mL bubble concentration was used and the acoustic amplitude was set to 70 kPa as that showed the strongest change in subharmonic. The relative subharmonic intensity, as determined in the ROI, is plotted in blue in Figure 6 for the first six decreasing SAP levels (100, 80, 60, 40, 20 and 0 mm Hg additional SAP, respectively). The intensities obtained from the 640 DAP-modulated frames at 60, 40, 20 and 0 mm Hg (Fig. 6c–f) were modulated by up to 4 dB, and this modulation followed the trend of the DAP (plotted in orange). This confirmed that the DAP has the same effect on subharmonic intensity in this co-propagation experiment as observed earlier during the cross-propagation

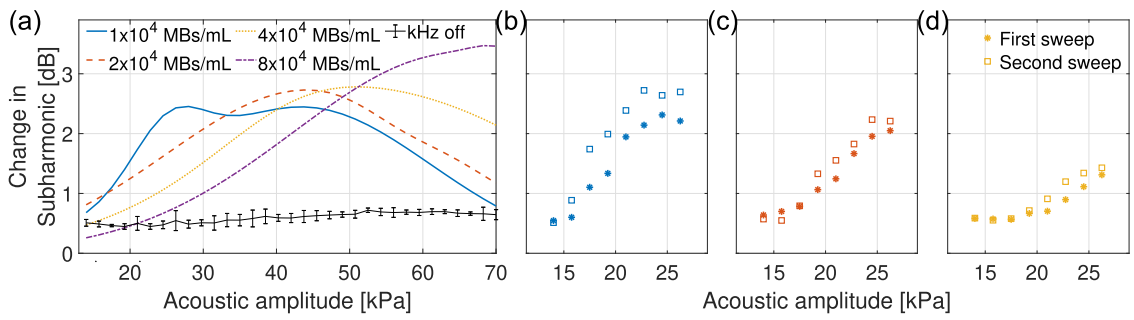

Figure 5. Subharmonic intensity change as a function of peak acoustic imaging pressure for four different bubble concentrations displayed by colored lines and the noise level recorded at ambient pressure in black (a). The colored lines were obtained from fitting a second-order Gaussian through individual measurements. Subharmonic intensity change as a function of acoustic pressure for the first (*solid stars*) and second (*empty squares*) acoustic amplitude sweep for the lowest three microbubble concentrations: (b) 1×10^4, (c) 2×10^4 and (d) 4×10^4 MBs/mL.

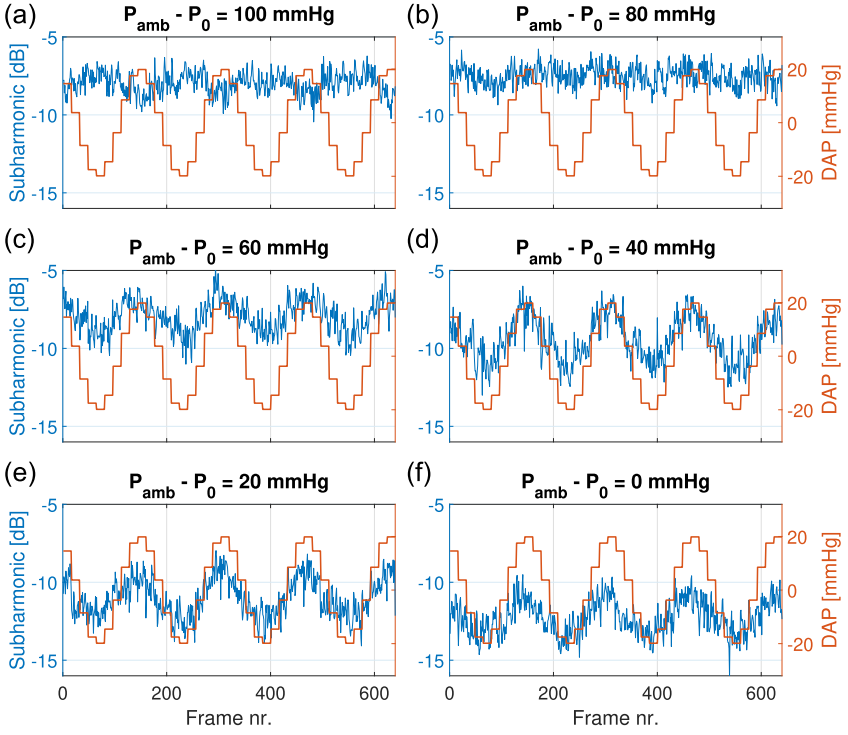

Figure 6. Subharmonic intensity as a function of frame number (*blue*) plotted together with the dynamically manipulated ambient pressure (*orange*) for decreasing static ambient pressures starting at (a) 100 mm Hg to (f) 0 mm Hg.

experiments. The tissue-mimicking material showed no subharmonic intensity or sensitivity, which confirmed that the microbubbles were responsible for the subharmonic signal. The subharmonic intensity at 100 mm Hg did not respond to the DAP, and the subharmonic intensity at 80 mm Hg had a weak response to the DAP of approximately 1 dB.

The relative subharmonic intensities are plotted as a function of the instantaneous ambient pressure (*i.e.*, SAP + DAP) for the entire SAP cycle in Figure 7. The same data are shown for all five experiments with fresh microbubble suspensions in Figure A.9. This shows foremost shows that the unmodulated reference subharmonic intensity (black squares in Fig. 7a) increased by 4 dB from 0 mm Hg to 60 mm Hg, then increased by 0.5 dB to 80 mm Hg, and finally decreased by 0.5 dB at 100 mm Hg. When the SAP was removed, the subharmonic intensity followed the same trajectory (dashed gray line in Fig. 7a and black diamond in Fig. 7d) down until 20

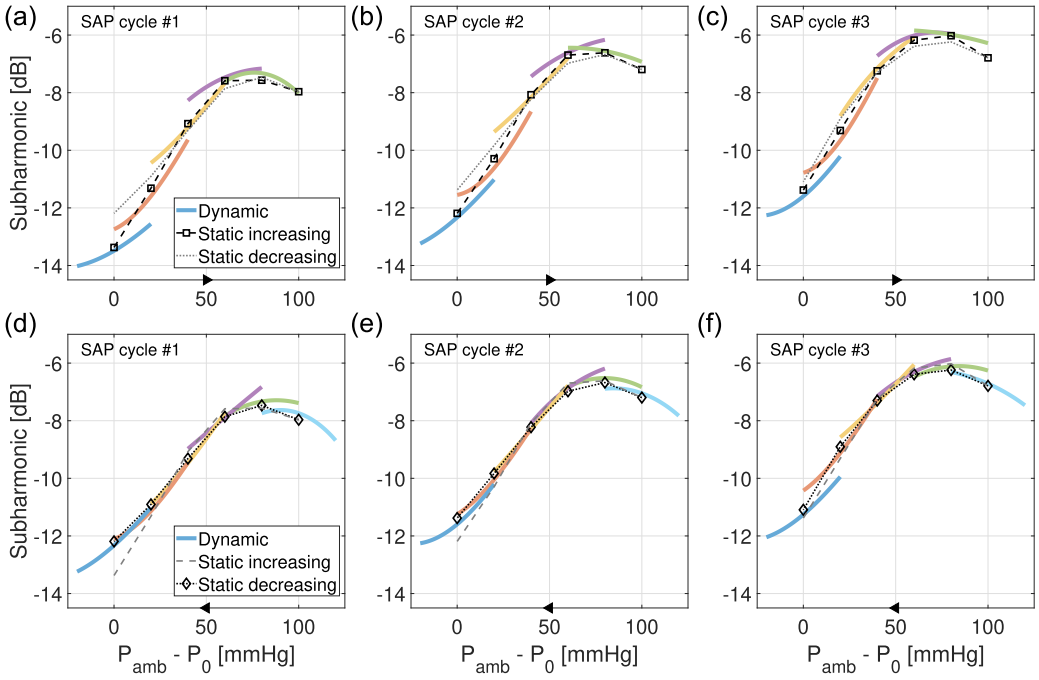

Figure 7. Relative subharmonic intensities as a function of instantaneous over-pressure P_{amb} - P_0 measured during (a–c) increasing static ambient pressure (SAP) and (d–f) decreasing SAP. (a and d) Correspond to the first SAP cycle, (b and e) with the second SAP cycle and (c and f) with the third SAP cycle. Reference subharmonic values (denoted 'Static') are shown by the dashed black line with square markers. Dynamic ambient pressure-modulated intensities are shown by the dashed colored lines.

mm Hg, but was 1 dB higher at 0 mm Hg. For the second and third SAP cycles (Figs. 7b, c, e, f), the subharmonic intensity as a function of static over-pressure followed the same trajectory as during the first SAP cycle, although the base subharmonic level increased by 1.5 dB. The same subharmonic trajectory as a function of static over pressure, and the same increase in subharmonic intensity of approximately 1.5 dB, was observed for the four repeat experiments, see Figure A.9B–E. This shows that the subharmonic sensitivity to ambient pressure is reversible. The deviation between the subharmonic intensity at 0 mm Hg measured before and after a complete SAP cycle decreased over each SAP cycle and was negligible in the third cycle.

The DAP-modulated subharmonic intensity (the lines colored blue at 0, orange at 20, yellow at 40, purple at 60, green at 80 and teal at 100 mm Hg in Fig. 7; 'Dynamic' was obtained by fitting a second-order polynomial through the 10 DAP-modulated subharmonic intensities, see Fig. A.8) generally matched well with the reference subharmonic intensities. The subharmonic sensitivity value in the SAP range of 0–60 mm Hg (Fig. A.8) was 0.49 dB/kPa, which was in line with [22] but lower than [23,24]. The correspondence between dynamic and static subharmonics was excellent, while the static over-pressure decreased (Fig. 7d–f) but the slope was slightly underestimated during the increase in static pressure (Fig. 7a–c).

Discussion

A dual-frequency ultrasound imaging technique was investigated that has the potential to measure relative pressure differences. It combines subharmonic CEUS imaging for pressure estimation with lower frequency radial modulation to calibrate the pressure sensitivity of the imaged microbubbles. This dynamic pressure sensitivity was compared with the pressure sensitivity following a static pressure change. The dynamic subharmonic sensitivity showed a good match with the static sensitivity, although a slight underestimation of the slope was observed during increasing SAP. The generally good correspondence between the dynamic and statically measured subharmonic intensities indicates that the subharmonic sensitivity to DAP is equivalent to SAP, making it possible to measure the relationship between subharmonic intensity and ambient pressure *in vivo* (*i.e.*, determine the dB/mm Hg value) in an imaging setting.

Although the sensitivity measured here was largely reversible, a slight change in subharmonic intensity at 0 mm Hg before and after the SAP cycle(s) was observed (Fig. 7). Another difference could be seen between the slope of the dynamic and static subharmonics while increasing the SAP (Fig. 7). Both these effects could be the result of diffusion-driven gas exchange that potentially alters the size and subharmonic behavior of the microbubbles between SAP levels. It would be interesting to see whether these differences are still seen in a pressurization cycle following a cardiac timescale of 1 Hz, instead of the static pressurization done here.

While dual-frequency imaging has been thoroughly investigated for its potential to enhance microbubble signal (radial modulation) [21,25–27], in this paper we proposed its use as a measurement method. Dual-frequency ultrasonic imaging for the purposes of measuring physical properties have been proposed before; *e.g.*, for measuring fat content through speed of sound changes. A strong limitation of such an approach is that the modulating pressure needs to be precisely known and has to be relatively high (400 kPa), which means that higher frequencies (700 kHz) that are more sensitive to attenuation are employed [28], thus limiting the quantitative value of the measurement. For the low-frequency wave used here attenuation was negligible [28], and thus it could be used to reliably relate subharmonic intensities to a difference in hydrostatic pressure irrespective of the imaged area.

While attenuation does affect the higher frequency imaging wave, and thus conventional SHAPE, by altering the driving force and resulting behavior of the microbubbles [22], this issue is bypassed in part by optimizing the acoustic intensity on a per-patient basis [16]. Although this protocol maximizes subharmonic sensitivity, it does not address the spatiotemporal variation of microbubbles in the body. This time dependency still poses a limiting factor, as the examination time is not always known *a priori*. It also limits the direct applicability in a medium different than blood [29], or when other agents are present in the blood [7]. Given this uncertainty in applicability and sensitivity values, an intrinsic calibration *via* dual-frequency ultrasound could help to enable widespread usage of minimally invasive pressure measurements in ultrasound imaging. It could achieve this by: (i) always providing quantitative pressure values, (ii) allowing it to be used in situations where it is currently is ambiguous (such as in the bladder [29]) and (iii) adding resilience to spatiotemporal variations in the imaged microbubbles.

The measurements as a function of SAP cycles shown in Figure 7 show an increase in subharmonics with ambient pressure from 0 to 60 mm Hg, and then a plateau at around 80 mm Hg followed by a slight decrease to 100 mm Hg. This tri-phasic subharmonic sensitivity behavior of SonoVue has been measured before [23,24,30–33], although other studies measured a strictly negative sensitivity (decreasing with SAP) from SonoVue [22,34]. This apparent inconsistency appears to be related to the imaging pressure amplitude [23,31] as the subharmonic sensitivity becomes negative for higher driving pressures (above 400 kPa [30,34]), which is more in line with the behavior as seen from other types of contrast agents [9]. High-amplitude driven subharmonics rely on compression-driven size changes of the gas core as opposed to the low-amplitude subharmonics, which are sensitive *via* lipid packing. The downside of these higher amplitude subharmonics is that they are prone to acoustic deflation [22], which could lead to irreversible changes, rendering it impossible to measure ambient pressure changes on the same microbubbles. However, high-amplitude subharmonics have been demonstrated *in vivo* [11,12,35] and may in fact be more resilient to changes from static pressurization [34]. Therefore, it would be worthwhile to investigate whether the dual-frequency strategy can calibrate the sensitivity of high-amplitude driven subharmonics.

Implications

The dual-frequency technique we investigated has the potential to allow quantitative local blood pressure difference measurements from CEUS imaging. However, this technique does not provide an absolute pressure measurement as the baseline pressure level is unknown. Although in principle this measurement technique could be applied wherever CEUS is applicable, we envision some practical implementations. One such implementation could be to quantify the pressure drop over an arterial stenosis by adjusting the DAP amplitude such that it bridges the difference in subharmonic intensity before and after the stenosis. Another implementation could be to measure the intra-cranial pressure by dynamically matching the subharmonic intensities of the intra-cranial and extra-cranial part of the ophthalmic artery, similar to the approach of two-depth transcranial Doppler [36] but without the need for pressurizing the tissue around the eye. To minimize the amplitude of the low-frequency wave (that could introduce adverse biological effects [37]), a strategy could be adopted that continuously measures the subharmonic sensitivity to DAP by transmitting a group of three pules, one at the negative and positive peaks of the LF wave, and one unmodulated reference frame. The sensitivity derived from the modulated frames could then be used to measure the pressure change from the current to the next reference frame. The downside of the dual-frequency technique proposed here is that it does require specialized hardware, namely a custom dual-frequency transducer or a low-frequency attachment for existing probes.

Conclusion

Subharmonic microbubble oscillations are responsive to ambient pressure, but deriving meaningful pressure estimations from subharmonic CEUS imaging is difficult as subharmonics also depend on

other factors. Here, we showed that a low-frequency ultrasound wave with a known acoustic amplitude can provide real-time feedback on the subharmonic sensitivity to ambient pressure. This can enable quantification of blood pressure differences from subharmonic CEUS imaging.

As a proof of principle of this dual-frequency technique, we combined a low-frequency single-element transducer with an imaging probe and imaged the effect of a static pressure cycle on the subharmonic scattering from a microbubble suspension. The results show a good match between the subharmonic sensitivity from the dynamic and from the static over-pressure.

Conflict of interest

The authors have no conflicts to disclose.

Acknowledgments

The work described in this article was funded by project Bubble-X of the research program Ultra-X-Treme (P17-32), financed by the Dutch Research Council (NWO). The authors thank Luxi Wei for suggesting sampling in space instead of in time. The authors also thank Michiel Manten, Stein Beekenkamp and Robin van Vlerken for fabrication of the experimental setup, and thank Robert Beurskens for helping with the design of the probe holder, all from Erasmus MC.

Data availability statement

The data that support the findings of this study are available from the corresponding author upon reasonable request.

Supplementary materials

Supplementary material associated with this article can be found in the online version at doi:10.1016/j.ultrasmedbio.2025.01.015.

References

[1] Fukumura D, Jain RK. Tumor microenvironment abnormalities: Causes, consequences, and strategies to normalize. J Cell Biochem 2007;101:937–49.
[2] McDonagh TA, Metra M, et al. 2021 ESC Guidelines for the diagnosis and treatment of acute and chronic heart failure. Eur Heart J 2021;42:3599–726.
[3] Tremblay-Darveau C, Williams R, Burns PN. Measuring absolute blood pressure using microbubbles. Ultrasound Med Biol 2014;40:775–87.
[4] Spiekhout S, Wang Y, Segers T, Kooiman K, Versluis M, Voorneveld J, De Jong N, Bosch JG. Ambient Pressure Sensitivity of Subharmonically Vibrating Single Microbubbles. https://doi.org/10.1016/j.ultrasmedbio.2025.01.016.
[5] Kwan JJ, Borden MA. Microbubble dissolution in a multigas environment. Langmuir 2010;26:6542–8.
[6] Kanbar E, Fouan D, Sennoga CA, Doinikov AA, Bouakaz A. Impact of filling gas on subharmonic emissions of phospholipid ultrasound contrast agents. Ultrasound Med Biol 2017;43:1004–15.
[7] Esposito C, Tzan K, Machado P, Forsberg F, Dave JK. The effect of mixing iodinated contrast media and ultrasound contrast agents on subharmonic signals. Ultrason Imaging 2024;46:130–4.
[8] Azami RH, Forsberg F, Eisenbrey JR, Sarkar K. Ambient pressure sensitivity of the subharmonic response of coated microbubbles: Effects of acoustic excitation parameters. Ultrasound Med Biol 2023;49:1550–60.
[9] Halldorsdottir VG, Dave JK, Leodore LM, Eisenbrey JR, Park S, Hall AL, et al. Subharmonic contrast microbubble signals for noninvasive pressure estimation under static and dynamic flow conditions. Ultrason Imaging 2011;33:153–64.
[10] Halldorsdottir V, Dave J, Eisenbrey J, Machado P, Zhao H, Liu J, et al. Subharmonic aided pressure estimation for monitoring interstitial fluid pressure in tumours *in vitro* and *in vivo* proof of concept. Ultrasonics 2014;54:1938–44.
[11] Lu H, Xu G, Wang Y, Yang H, Li D, Huang L, et al. Correlation between portal vein pressure and subharmonic scattering signals from SonoVue microbubbles in canines. Ultrasound Med Biol 2023;49:203–11.
[12] Forsberg F, Piccoli CW, Sridharan A, Wilkes A, Sevrukov A, Ojeda-Fournier H, et al. 3D harmonic and subharmonic imaging for characterizing breast lesions: A multicenter clinical trial. J Ultrasound Med 2022;41:1667–75.
[13] Forsberg F, Gupta I, Machado P, Shaw CM, Fenkel JM, Wallace K, et al. Contrast-enhanced subharmonic aided pressure estimation (SHAPE) using ultrasound imaging with a focus on identifying portal hypertension. J Vis Exp 2020;166:e61817.
[14] Dave JK, Kulkarni SV, Pangaonkar PP, Stanczak M, McDonald ME, Cohen IS, et al. Non-invasive intra-cardiac pressure measurements using subharmonic-aided pressure estimation: Proof of concept in humans. Ultrasound Med Biol 2017;43:2718–24.
[15] Gupta I, Eisenbrey J, Stanczak M, Sridharan A, Dave JK, Liu J-B, et al. Effect of pulse shaping on subharmonic aided pressure estimation in vitro and *in vivo*. J Ultrasound Med 2017;36:3–11.
[16] Dave JK, Halldorsdottir VG, Eisenbrey JR, Merton DA, Liu J-B, Machado P, et al. On the implementation of an automated acoustic output optimization algorithm for subharmonic aided pressure estimation. Ultrasonics 2013;53:880–8.
[17] Faez T, Renaud G, Defontaine M, Calle S, de Jong N. Dynamic manipulation of the subharmonic scattering of phospholipid-coated microbubbles. Phys Med Biol 2011;56:6459–73.
[18] Masoy S-E, Standal O, Nasholm P, Johansen T, Angelsen B, Hansen R. SURF imaging: *In vivo* demonstration of an ultrasound contrast agent detection technique. IEEE Trans Ultrason Ferroelectr Freq Control 2008;55:1112–21.
[19] Chen P, Pollet AM, Panfilova A, Zhou M, Turco S, den Toonder JM, et al. Acoustic characterization of tissue-mimicking materials for ultrasound perfusion imaging research. Ultrasound Med Biol 2022;48:124–42.
[20] Havlice J, Taenzer J. Medical ultrasonic imaging: An overview of principles and instrumentation. Proc IEEE 1979;67:620–41.
[21] Jing B, Lindsey BD. Very low frequency radial modulation for deep penetration contrast-enhanced ultrasound imaging. Ultrasound Med Biol 2022;48:530–45.
[22] Andersen KS, Jensen JA. Impact of acoustic pressure on ambient pressure estimation using ultrasound contrast agent. Ultrasonics 2010;50:294–9.
[23] Nio AQX, Faraci A, Christensen-Jeffries K, Raymond JL, Monaghan MJ, Fuster D, et al. Optimal control of SonoVue microbubbles to estimate hydrostatic pressure. IEEE Trans Ultrason Ferroelectr Freq Control 2020;67:557–67.
[24] Li F, Li D, Yan F. Improvement of detection sensitivity of microbubbles as sensors to detect ambient pressure. Sensors 2018;18:4083.
[25] Bouakaz A, Versluis M, Borsboom J, De Jong N. Radial modulation of microbubbles for ultrasound contrast imaging. IEEE Trans Ultrason Ferroelectr Freq Control 2007;54:2283–90.
[26] Angelsen BA, Hansen R. 7A-1 SURF imaging – A new method for ultrasound contrast agent imaging. In: Paper presented at: 2007 IEEE Ultrasonics Symposium. October 28–31; 2007. p. New York, NY, USA531–41.
[27] Yang J, Cherin E, Yin J, Newsome IG, Kierski TM, Pang G, et al. Characterization of an array-based dual-frequency transducer for superharmonic contrast imaging. IEEE Trans Ultrason Ferroelectr Freq Control 2021;68:2419–31.
[28] Treeby BE, Zhang EZ, Thomas AS, Cox BT. Measurement of the ultrasound attenuation and dispersion in whole human blood and its components from 0-70 MHz. Ultrasound Med Biol 2011;37:289–300.
[29] Kalayeh K, Fowlkes JB, Chen A, Yeras S, Fabiilli ML, Claflin J, et al. Pressure measurement in a bladder phantom using contrast-enhanced ultrasonography: A path to a catheter-free voiding cystometrogram. Invest Radiol 2023;58:181–9.
[30] Frinking PA, Gaud E, Brochot J, Arditi M. Subharmonic scattering of phospholipid-shell microbubbles at low acoustic pressure amplitudes. IEEE Trans Ultrason Ferroelectr Freq Control 2010;57:1762–71.
[31] Nio AQX, Faraci A, Christensen-Jeffries K, Eckersley RJ, Monaghan MJ, Raymond JL, et al. The subharmonic amplitude of SonoVue increases with hydrostatic pressure at low incident acoustic pressures. In: Paper presented at: 2017 IEEE International Ultrasonics Symposium (IUS). September 5–9; 2017. p. Washington DC, USA. p. 1–4.
[32] Gupta I, Eisenbrey JR, Machado P, Stanczak M, Wallace K, Forsberg F. On factors affecting subharmonic-aided pressure estimation (SHAPE). Ultrasonic Imaging 2019;41:35–48.
[33] Mayer H, Kim GW, Machado P, Eisenbrey JR, Vu T, Wallace K, et al. Investigation into the subharmonic response of three contrast agents in static and dynamic flow environments using a commercially available diagnostic ultrasound scanner. Ultrasound Med Biol 2024;50:1731–8.
[34] Azami RH, Forsberg F, Eisenbrey JR, Sarkar K. Acoustic response and ambient pressure sensitivity characterization of SonoVue for noninvasive pressure estimation. J Acoust Soc Am 2024;155:2636–45.
[35] Halldorsdottir VG, Dave JK, Marshall A, Forsberg AI, Fox TB, Eisenbrey JR, et al. Subharmonic-aided pressure estimation for monitoring interstitial fluid pressure in tumors: calibration and treatment with paclitaxel in breast cancer xenografts. Ultrasound Med Biol 2017;43:1401–10.
[36] Ragauskas A, Daubaris G, Dziugys A, Azelis V, Gedrimas V. Innovative non-invasive method for absolute intracranial pressure measurement without calibration. Intracranial Pressure and Brain Monitoring XII. Vienna: Springer-Verlag; 2005. p. 357–61.
[37] Ahmadi F, McLoughlin IV, Chauhan S, ter Haar G. Bio-effects and safety of low-intensity, low-frequency ultrasonic exposure. Prog Biophys Mol Biol 2012;108:119–38.